Cumhuriyet Sci. J., 43(1) (2022) 137-145
DOI: https://doi.org/10.17776/csj.990817

Cumhuriyet Science Journal

| csj.cumhuriyet.edu.tr | Founded: 2002 ISSN: 2587-2680 e-ISSN: 2587-246X Publisher: Sivas Cumhuriyet University

The Investigation of Photovoltaic and Electrical Properties of Bi Doped CTS/Si Hetero-Junction Structure for the Solar Cell Application

Serap Yiğit Gezgin[2,a], Amina Houimi[1,b], Bedrettin Mercimek[3,c], Hamdi Şükür Kiliç[2,4,5,d,*]

[1]*Department of Nano-technology and developed materials, Faculty of Science, University of Selçuk, 42031, Konya, Türkiye.*
[2]*Department of Physics, Faculty of Science, University of Selçuk, 42031, Konya, Türkiye.*
[3]*Department of Chemistry Education, Faculty of Ahmet Keleşoğlu Education, Necmettin Erbakan University, 42090, Konya, Türkiye.*
[4]*Directorate of High Technology Research and Application Center, University of Selçuk, 42031, Konya, Türkiye.*
[5]*Directorate of Laser Induced Proton Therapy Application and Research Center, University of Selçuk, 42031, Konya, Türkiye.*
**Corresponding author*

Research Article

History
Received: 05/09/2021
Accepted: 05/03/2022

ABSTRACT

In this study, we have produced Cu-Sn-S (CTS) and Bi doped CTS powder composite structures by mixing CuS and SnS_2 powders and adding %3 Bi into CuS-SnS_2 (1:1) powder mixture. These raw powders were mixed and milled by a ball milling device and then CTS and Bi doped CTS target pellets have been produced by cold pressing using a mold prepared in special dimensions. The morphology and crystal structure of target pellets have analysed by SEM and XRD techniques. The target pellets contain different crystalline phases such as: Cu_2SnS_3, $Cu_2Sn_3S_7$, $Cu_4Sn_7S_{16}$ and SnS. It has been experienced that Bi doped CTS target pellet has better morphology compared to CTS target pellet. Using PLD technique, the target pellets have been ablated by laser beam to deposited thin film on soda lime glass substrates. According to AFM analysis, the particle size that forms Bi doped CTS thin film is larger than that of CTS thin film. Bi doped CTS thin film has poor crystal structure, while the pure CTS thin film were amorphous. The band gap of Bi doped CTS thin film is slightly lower than that of CTS thin film. While the produced Ag/CTS/Si/Al hetero-junction has not shown diode feature, Ag/Bi dop CTS/Si/Al hetero-junction has exhibited photovoltaic behaviour. The ideality factor, the barrier height, serial resistivity of Ag/Bi dop CTS/Si/Al hetero-junction have been calculated by the conventional $J-V$, Cheung-Cheung and Norde methods in the darkness and under the illumination (AM 1.5 solar radiation in 80 mW/cm^2). The photovoltaic parameters of the hetero-junction have been determined and interpreted in detail in this article.

Keywords: Target pellet, Doped, Bi doped CTS, Thin film, Ball milling, PLD.

[a] *serap.gezgin@selcuk.edu.tr* *https://orcid.org/0000-0003-3046-6138*
[b] *aminahouimi@gmail.com* *https://orcid.org/0000-0002-2621-2250*
[c] *bedrettinmercimek@gmail.com* *https://orcid.org/0000-0002-3407-6906*
[d] *hamdisukurkilic@selcuk.edu.tr* *https://orcid.org/0000-0002-7546-4243*

Introduction

In recent years, many studies have been actualised on Cu-Sn-S (CTS) system consisting of ternary components such Cu_2SnS_3, Cu_4SnS_4, Cu_3SnS_4, $Cu_2Sn_3S_7$, $Cu_4Sn_7S_{16}$ [1-4] for thin film solar cells. Cu_2SnS_3, which has the most stable structure among these ternary components, is a p-type semiconductor in high absorption coefficient, 0.9-1.35 eV direct band gap and it also consists of non-toxic and low cost elements. It is foreseen that use of CZTS (Cu_2ZnSnS_4) as an absorber layer will be replaced in thin film solar cell. In order to realise this, advanced studies have been actualised on the optical, crystal and morphological properties of Cu_2SnS_3 material. At this point, a significant increase has been succeed in the efficiency of solar cells by doping Ge (6%) and Na (4.6%) atoms into Cu_2SnS_3 [5]. Among the prospective doping elements, Bismuth (Bi) is a V group element that offers an acceptor dopant property to p-type semiconductor material. Bi element has been used as a dopant for p-type materials such as CIS ($CuInS_2$), CIGS ($CuInGaS_2$) and CZTS resulting in an increase in particle size of materials, passivation of the donor defects, improvement in their crystal structure, and an increase in the number of charge carriers [6-8]. Furthermore, these parameters have been improved the open circuit voltage (V_{oc}), filling factor (FF) and power conversion efficiency (η) of produced solar cells [9]. With this point of view, Antimony (Sb) element, which shares the same group element with Bi atom, has developed the crystal structure of Cu_2SnS_3 [10] showing that Bi doping element can increase the efficiency of Cu_2SnS_3 based solar cell to be produced.

The deposition techniques such as electron beam evaporation, sputtering and pulse laser deposition (PLD) techniques have been used to produce Cu_2SnS_3 thin film [5]. PLD is a simple system consisting of vacuum chamber and laser system. PLD system is a very power full technique serving very prominent advantageous for stoichiometric transfer and homogeneous thin film growth. By changing PLD parameters such as laser fluency, background gas pressure, laser wavelength and substrate temperature, we can adjust the optical, crystalline, morphological and electrical properties of the growth thin film [11-13].

In this study, in order to produce Bi doped CTS material, we have added Bi powder into CTS powder mixture, mixed it by a ball milling technique and then we have formed target pellets of pure CTS and Bi doped CTS

components. Bi doped CTS target pellet has been ablated by a laser beam and its thin film has been deposited on n-Si wafer and soda lime glass (SLG) substrate using PLD technique. We have performed production and characteristic analyses of CTS and Bi doped CTS target pellets and their thin films. Al and Ag contacts have been coated on the rear side of Si wafer and Bi doped CTS thin film in produced Si/Bi doped CTS hetero-junction, respectively. $J-V$ graphs of Ag/Bi doped CTS/Si/Al hetero-junctions were determined at dark and under illumination conditions and their electrical and photovoltaic properties have also been investigated.

Experimental

Produce of Cts, Bi Doped Cts Target Pellets and Ag/Bi Doped Cts (And Non Doped Cts)/Si/Al Hetero-Junctions

CTS and Bi doped CTS powder components have been formed by Cu_xS-SnS_2 powder mixture and adding %3 Bi into Cu_xS-SnS_2 (1:1) powder mixture, respectively (Fig. 1a). The raw powders have been mixed and milled for 9 hour by a ball milling device shown in Fig 1b. CTS and Bi doped CTS powder mixture have been annealed at 600 °C for 1 hour in a quartz tube furnace under vacuum. The target pellets (Fig 1e) have been produced by cold pressing the resulted powders (Fig 1d) using a special mould (Fig 1c). The diameter and thickness of the target pellet are 12 mm and 2mm, respectively. The target pellets have been annealed at 700°C for 6 hours under argon ambient gas environment.

Before starting the thin film production process, SLG and silicon wafer substrate were cleaned. After cleaning the SLGs with foamy soap, they were soaked in acetone and isopropyl alcohol for 15 minutes *via* ultrasonic bath, respectively. Si wafer was first cleaned with foamy soap and then kept in HF: distilled water (1:24) solution mixture for 2 minutes to remove the oxide layer. Then, Si wafer was soaked in distilled water for 5 minutes. SLG and Si wafers were dried with nitrogen gas jet just before the deposition process started. n-Si wafer used to form hetero-junction, has 10 Ω.cm resistance, 500 µm thickness and (100) crystalline orientation.

In order to produce thin film with PLD technique, the target-substrate distance was adjusted to 45mm. The pressure of vacuum chamber was reduced down to 3×10^{-6} mbar. Pure CTS and Bi doped CTS target pellets were ablated by laser beam using 1.6 J/cm^2 laser fluency and 1064 nm wavelength for 90 minutes.

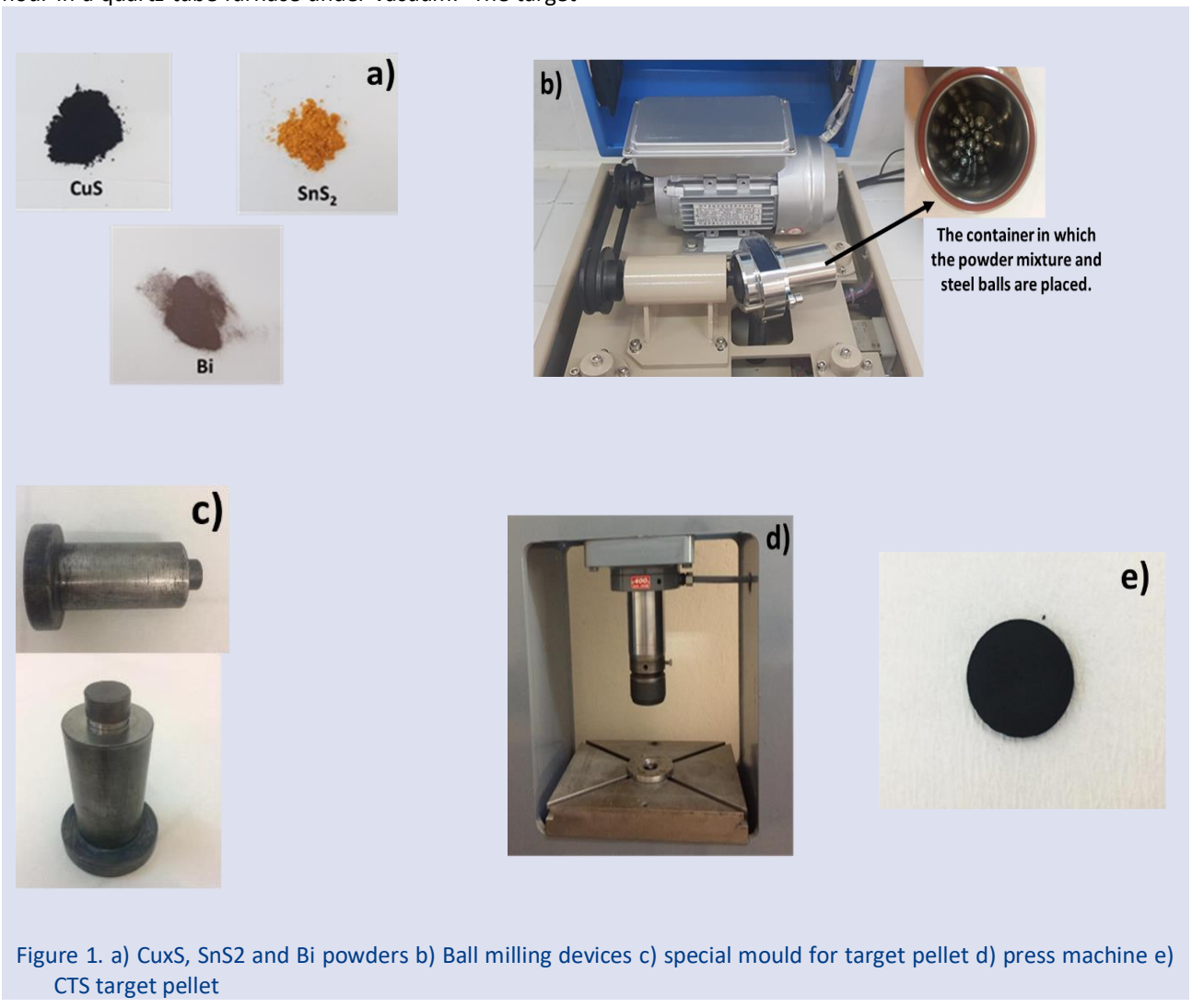

Figure 1. a) CuxS, SnS2 and Bi powders b) Ball milling devices c) special mould for target pellet d) press machine e) CTS target pellet

The thin films were deposited on SLG and the front face of n-Si wafer at room temperature *via* the plasma in Fig 2a. Al metal contacts were deposited on rear face of n-Si wafer using Physical Vapour Deposition (PVD) and then, CTS and Bi doped thin films were placed next to 50 mg of sulphur powder in a quarts tube and annealed at 400°C temperature under vacuum. Ag finger front contact was deposited on Bi doped CTS (and CTS) thin films by PVD technique, forming Ag/Bi doped CTS (and non doped CTS)/Si/Al heterojunctions. The thickness of back (Al) and front (Ag) contacts was measured to be 150 nm. The active area and size of the heterojunction diodes, which are 0.2 cm^2 and 1 cm^2, respectively.

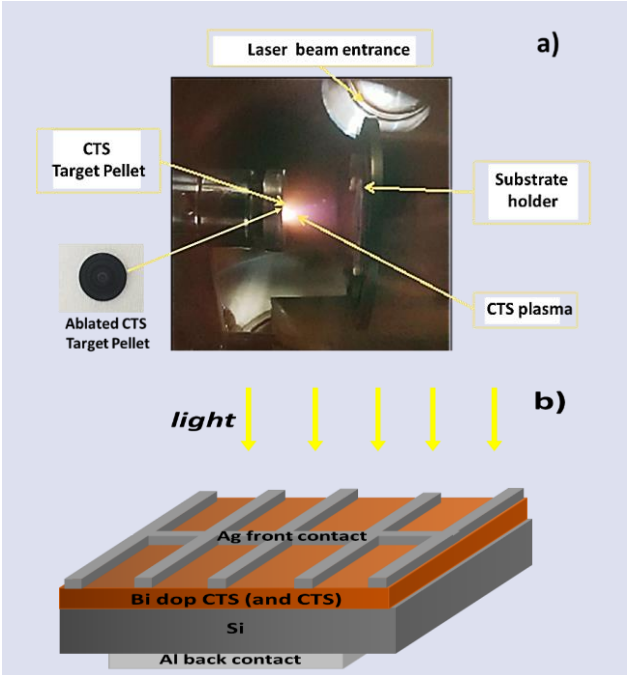

Figure 2. a) Photograph of CTS plasma and b) Ag/Bi doped CTS (and CTS)/Si/Al heterojunctions diagram

Material Characterization

The crystal structure and morphology of CTS and Bi doped CTS target pellets have been determined by XRD (X-Ray Diffraction) and SEM (Scanning Electron Microscopy) analyses, while the crystal, optical and morphological properties of their thin films structures have been determined by XRD, UV-vis spectra and AFM (Atomic Force Microscopy), respectively. $J-V$ characteristics of pure and Bi doped CTS/Si hetero-junctions were obtained in the darkness and the illumination conditions. The ideality factor (n), barrier height (Φ_B) and series resistance (R_s) have been calculated by conventional $J-V$, Cheung-Cheung, Norde methods and V_{oc}, J_{sc}, FF and η photovoltaic (PV) parameters have been obtained.

Discussion

XRD Analysis of CTS and Bi Doped CTS Target Pellets

Fig 3a and 3b show XRD Spectra of CTS and Bi doped CTS target pellets. Both target pellets contain different ternary phases of Cu-Sn-S sulphides, such as; Cu_2SnS_3 (JCPDS 00-027-0198), Cu_3SnS_4 (JCPDS 00-036-0218), $Cu_2Sn_3S_7$ (JCPDS 00-039-0970) and $Cu_4Sn_7S_{16}$ (JCPDS 01-089-4713), in addition one binary phase SnS (JCPDS 00-039-0354) phases [1-3, 5, 14-17]. These phases indicate that the target pellets have been found as Sn rich [4, 13, 16, 18, 19]. At temperatures above 400°C, the formation of SnS phase is probable [20] leading to an obvious SnS peak at the XRD diagram at both pure and doped CTS pellet targets. Also, it is likely for SnS phase to appear at Sn rich precursors [16, 21, 22]. However, the crystal structure of CTS target pellet has been weaken by the addition of the Bi atom [23-26]. We have also noticed a decrease in the density of peaks referring to SnS phase. Addition of Bi atom into CTS as a dopant can cause undesirable defects in CTS and it may cause deterioration of the crystal structure. Furthermore, Bi atoms (117 pm) are more likely to occupy Cu (91 pm), Sn (83 pm) and S (51 pm) vacancies. Since the ionic radius of Bi atoms is higher than that of other atoms, it can lead to surface strain, which adversely affects the crystal structure. Therefore, when Bi atoms are doped into CTS target pellet, the crystal structure of CTS target pellet can be weakened.

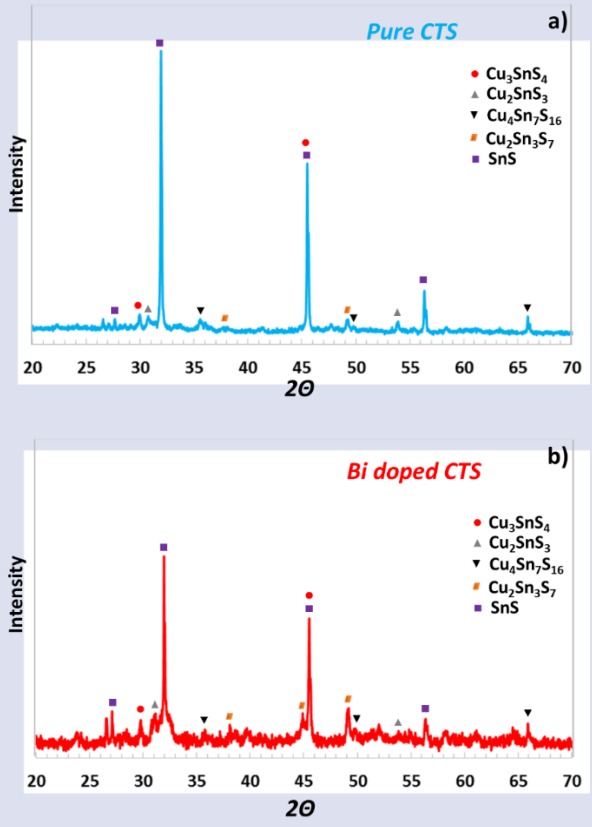

Figure 3. XRD spectrums of a) CTS and b) Bi doped CTS target pellets

The crystalline size of CTS target pellets have been obtained using Scherrer equation (eq.1):

$$D = 0.94\lambda/\beta cos\theta \quad (1)$$

Where D is the size of crystalline, λ is wavelength of X-Ray, β is full-width at half-maximum of diffraction peak and θ is Bragg diffraction angle. The main crystalline size of CTS and Bi doped CTS target pellets, which were calculated to be 76.24 nm and 59.08 nm using Scherrer equation, respectively. Due to the possibility of surface strain, the crystalline size of the Bi-doped CTS target pellet is smaller than the crystalline size of the CTS target pellet.

Morphologic Analyses of CTS and Bi Doped CTS Target Pellets

Bi doped CTS target pellet consists of larger particles compared to CTS target pellets, according to SEM images given in Fig. 4a and 4b. The reason behind this increase can be explained by the possibility of Bi (117 pm) atom occupying Sn (83 pm) and S (51 pm) vacancies and can cause an enlargement in the particle size. Furthermore, Bi doped CTS target pellet indicates more homogeneous and uniform particle distribution compared to CTS target pellet through Bi doping. Thus, an ideal laser ablation can be achieved using Bi doped CTS target pellet with its the smoother morphological structure.

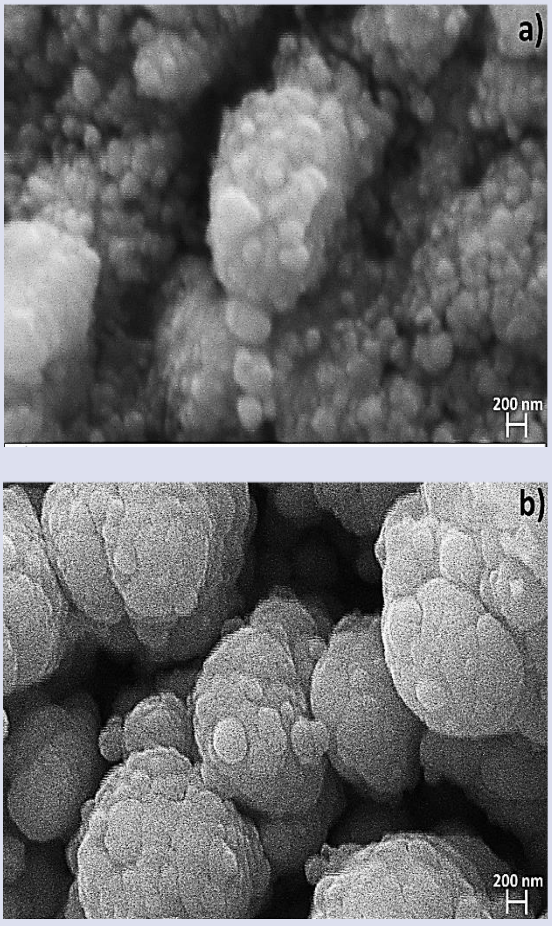

Figure 4. SEM images of a) CTS and b) Bi doped CTS target pellets

XRD Analysis of CTS and Bi Doped CTS Thin Films

XRD spectra of CTS and Bi doped CTS thin films are shown in Fig. 5. Bi doped CTS thin film has a very poor crystalline structure while CTS thin film is amorphous. Similar to the target pellet, a peak with a very low intensity was formed at 2θ= 32° indicating SnS phase [27] in XRD pattern of Bi doped CTS thin film. The cause of the amorphous structure of pure CTS thin film can be based to the fact that the CTS target pellet is not uniform and inhomogeneous compared to Bi doped CTS target pellet, and therefore, an ideal laser ablation process cannot be achieved. Annealing of Bi doped CTS thin film at low sulfurization temperature can cause a poor crystalline structure of thin film. In addition, Bi doped CTS thin film can be exposed to the wetting problem as it grown on Si wafer surface at higher sulfurization temperature and it can't completely cover the surface of Si wafer [28, 29]. Therefore, high annealing temperature is not preferred.

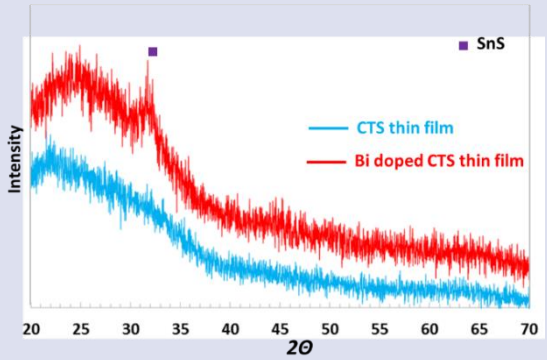

Figure 5. XRD spectrum of a) CTS and b) Bi doped CTS target films

Morphologic Analyses of CTS and Bi Doped CTS Thin Films

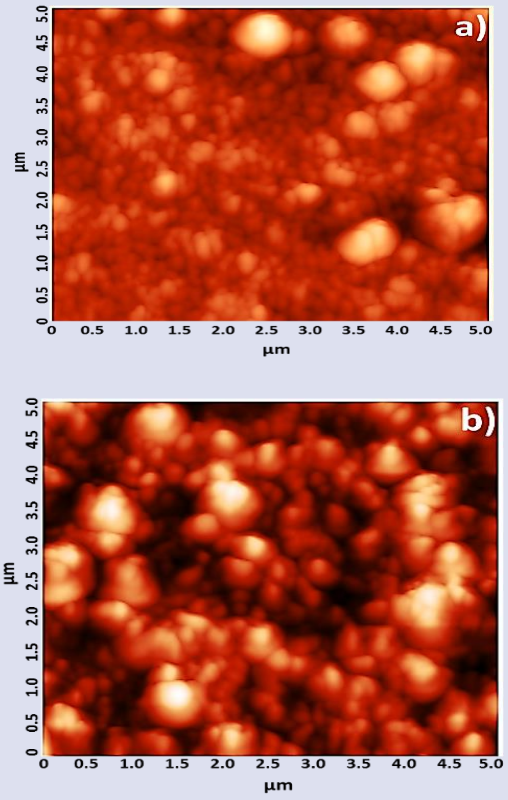

Figure 6. AFM images (in 5µm×5µm area) of a) CTS and b) Bi doped CTS thin films

AFM images of CTS and Bi-doped CTS thin films in 420 nm thickness are given in Fig 6a and 6b, respectively. The particle size of Bi doped CTS thin film is larger than that of CTS thin film. The fact that Bi atom (117 pm) can occupy Cu (68 pm) and S (51 pm) vacancies and then increase the particle size of Bi doped CTS thin film. The large particle size of Bi doped CTS thin film causes the reduction of the numbers of grain boundaries and the passivation of defects and traps within the boundaries. This provides some improvement in the crystal structure of Bi doped CTS thin film compared to pure CTS thin film [11, 30].

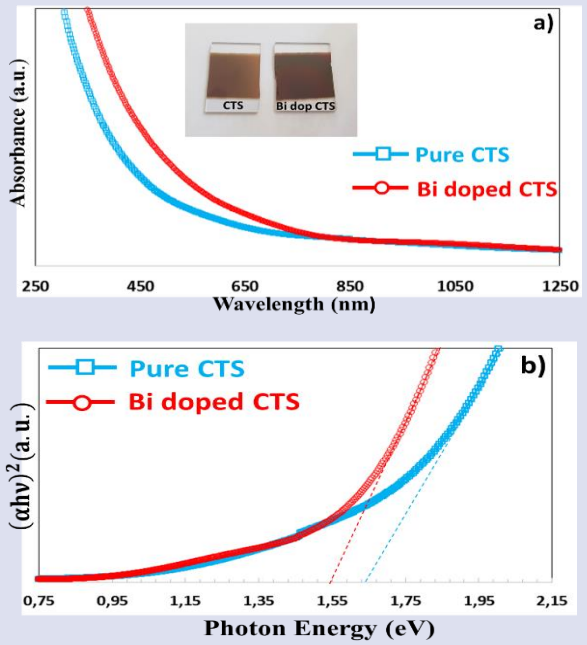

Figure 7. a) Absorbance spectrum (the photograph of CTS and Bi doped CTS in small squares) and b) Tauc plot of CTS and Bi doped CTS thin films

Bi doped CTS thin film absorbs slightly more light than CTS thin films, according to absorbance spectra shown in Fig. 7a. As shown in AFM image in Fig 6b, Bi atom has increased the particle size of Bi doped CTS thin film causing more light absorption. In addition, according to the photographs of CTS and Bi doped CTS thin films have been given in the small square in Fig. 7a, it appears that Bi doped CTS thin film is darker than CTS thin film and it can be foreseen that Bi doped CTS thin film can absorb more photons.

The band gaps of thin films have been calculated by Tauc Eq (2) expressed below:

$$(\alpha hv)^2 = A\left(hv - E_g\right)^{1/2} \quad (2)$$

where A, hv, E_g are a constant, the photon energy and the band gap of thin film, respectively. The band gaps of CTS and Bi doped CTS thin films have been determined as 1.64 eV and 1.55 eV from Tauc graph in Fig. 7b, using Eq (1), respectively. The photon absorption of Bi doped CTS thin film is slightly higher since its band gap is slightly lower. The band gap of Bi doped CTS thin film is more consistent with the value has been reported in the literature [31, 32].

The electrical characteristics of Ag/Bi doped CTS/Si/Al hetero-junctions in darkness and under illumination

Since the crystal structure of CTS thin film is amorphous, there are excessive defects and traps in this thin film structure. Because the charge carriers are recombined in these traps and defects, Ag/CTS/Si/Al hetero-junction could not show any diode features.

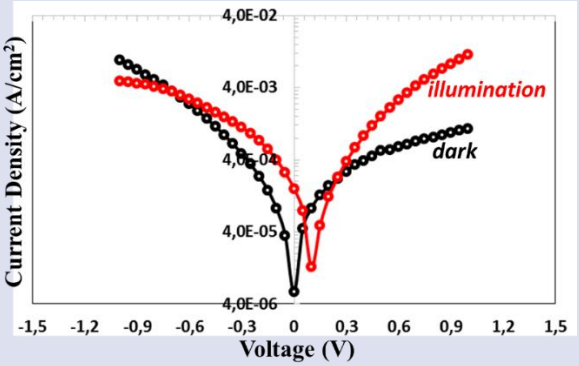

Figure 8. The logarithmic $J-V$ characteristic of Ag/Bi doped CTS/Si/Al heterojunction in the darkness and the illumination

However, Ag/Bi doped CTS/Si/Al hetero-junction has exhibited PV behaviour according to the logarithmic $J-V$ characteristics shown in Fig 8. The rectification ratio (RR) of a diode, which is expressed by Eq (3):

$$RR = \frac{I_F(+V)}{I_R(-V)} \quad (3)$$

Where, I_F is forward current in +1V, I_R is reverse current in -1V. Rectification rate of Bi doped CTS hetero-junction ($RR = 2.34$) under the darkness is higher than the rectification ratio ($RR = 0.11$) of the hetero-junction in the light. The increase in forward current due to photo-excited electron-hole pair formation lead to a better rectification behaviour of the hetero-junction [33]. However, the weak crystalline structure of Bi doped CTS thin film and the large number of defects and traps in its crystal structure cause more recombination of the charge carriers. Therefore, the rectification rates of the hetero-junction are low in the darkness and under the illumination.

The current of a diode is determined by Eq (4) in thermionic emission theory,

$$I = I_0[exp(qV/nkT) - 1] \quad (4)$$

V is applied forward bias voltage applied, I_o is saturation current, n is the ideality factor, q is electric charge, T is the absolute temperature and k is Boltzman constant. Ideality factor of a diode is given by Eq (5):

$$n = \frac{q}{kT}\frac{dV}{d(lnI)} \quad (5)$$

The ideality factor is determined by the drawn straight line in forward bias region in the logarithmic $J-V$ graph

seen in Fig 8. The ideality factors of the hetero-junction in darkness and the illumination conditions have been calculated to be $n_{dark} = 3.71$ and $n_{illum.} = 3.36$, respectively. The ideality factors of the hetero-junction in both environment conditions have been found to be rather high [34]. The reasons behind it might be referred to the leakage current and dangling-bonds that can occur at the interfaces of the depletion region where the recombination of charge carriers is high due to the existence of defects, traps and interface states formed due to the poor crystalline of Bi doped CTS thin film [11, 35, 36].

The barrier height (Φ_b) of a diode is obtained by using the following equation:

$$\Phi_b = \frac{kT}{q} ln\left(\frac{AA^*T^2}{I_o}\right) \quad (6)$$

A and A* are the active area of diode and Richardson constant (112 A cm^{-2}K^{-2} to n-Si), respectively. I_o saturation current is determined by the straight line drawn intersects y-axis of the reverse bias region in the logarithmic $J-V$ characteristic in Fig 8. The barrier heights of Bi doped CTS thin film in darkness and illumination conditions have been found to be $\Phi_{b(dark)} = 0.60$ eV and $\Phi_{b(illum.)}$=0.56 eV, respectively. The photo current result in that a decrease in both the ideality factor and barrier height of Bi doped CTS hetero-junction due to the photo excited charge carriers under illumination conditions [35, 37].

Serial resistance of a diode has been calculated using $R_s = \frac{\Delta V_{forward\ bias\ voltage}}{\Delta I_{forward\ bias\ current}}$ formula for the forward bias region of the logarithmic J-V curve [38]. We have obtained $R_s - V$ curve given in Fig. 9 using this formula and determined the saturated value of R_s serial resistances at high voltage.

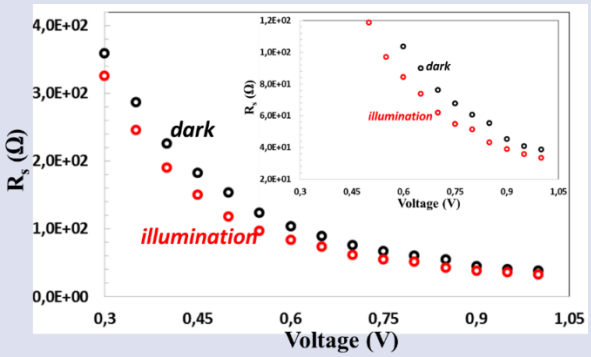

Figure 9. $R_s - V$ curve of Bi doped CTS hetero-junction in the darkness and the illumination

R_s values have been determined to be 38.84Ω and 33.57 Ω in the darkness and the illumination conditions. Electrons excited by the photon in the valence band of Bi doped CTS have been transmitted to the conduction band under the illumination conditions and cause the formation of charge carriers, thus the series resistance has been reduced [39, 40].

Table 1. The electrical parameters of Ag/Bi doped CTS/Si/Al hetero-junction in the darkness and the illumination

Bi doped CTS/Si hetero-junction	J-V Method			Cheung Cheung Method				Norde Method	
	dln(J)-V			dV/dln(J)-J		H(J)-J		F(V)-V	
	n	$R_s(\Omega)$	Φ_b(eV)	n	$R_s(\Omega)$	$R_s(\Omega)$	Φ_b(eV)	$R_s(\Omega)$	Φ_b (eV)
Darkness	3.71	38.84	0,60	6.68	17.49	21.91	0.61	49.63	0.65
Illumination	3.36	33.57	0.56	5.37	20.28	23.49	0.63	43.63	0.70

n, R_s and Φ_b parameters have been calculated by Cheung-Cheung method, Norde Method as well as the conventional J-V method and the result are presented in Table 1. Cheung-Cheung functions have been expressed by Eq 7), Eq (8) and Eq (9):

$$\frac{dV}{d(lnI)} = IR_s + n\left(\frac{kT}{q}\right) \quad (7)$$

$$H(I) = V - \left(\frac{nkT}{q}\right) ln\left(\frac{I}{AA^*T^2}\right) \quad (8)$$

$$H(I) = IR_s + n\Phi_b \quad (9)$$

$dV/d(\ln J) - J$ and $H(J) - J$ characteristics of Bi doped CTS hetero-junction are given in Fig 10a and 10b, respectively. y-axis intercept and the slope of $dV/d(\ln J) - J$ graphic obtained by Eq (7) show nkT/q and IR_s ,respectively. The ideality factors of the hetero-junction have been calculated to be $n_{dark} = 6.68$ and $n_{illum.} = 5.37$, while the serial resistances have been calculated to be $R_{s(dark)} = 17.49\Omega$ and $R_{s(illum.)} = 20.28\Omega$ in the darkness and the under illumination conditions, respectively. The ideality factors and serial resistitance determined by $dV/d(\ln J) - J$ characteristics are higher compared to that calculated by the conventional $J - V$ characteristics.

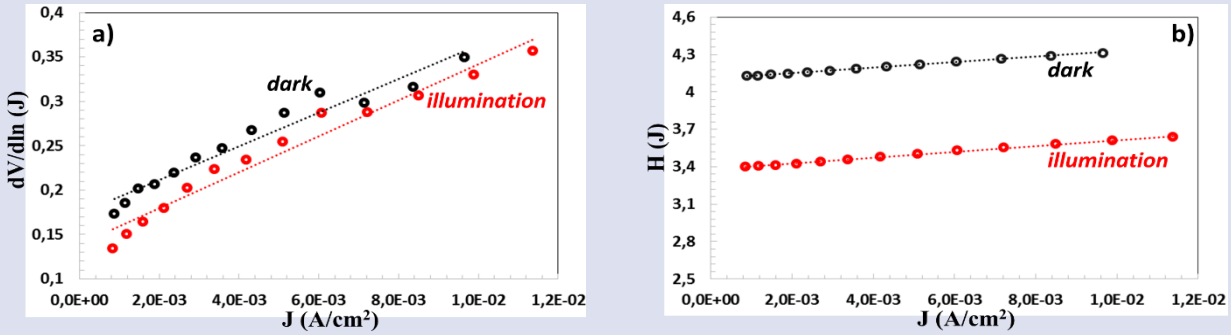

Figure 10. a) $dV/d(\ln J) - J$ and b) $H(J) - J$ curves of Bi doped CTS hetero-junctions in darkness and the illumination

y-axis intercept and the slope of $H(J) - J$ graphic obtained by Eq (8) present $n\Phi_b$ and IR_s in Eq (9). The serial resistance of Bi doped CTS hetero-junction have been calculated to be $R_{s(dark)} = 21.91\Omega$ and $R_{s(illum.)} = 23.49\Omega$, while its barrier height have been calculated to be $\Phi_{b(dark)} = 0.61$ eV and $\Phi_{b(illum.)} = 0.63$ eV in the darkness and the illumination conditions, respectively. R_s values obtained by $H(J) - J$ characteristic have been found to be slightly higher than that obtained by $dV/d(\ln J) - J$ characteristics. However, R_s values obtained by $H(J) - J$ characteristics have been found to be lower than that of the conventional $J - V$ characteristics. The ideality factors and serial resistance calculated by both conventional $J - V$ and Cheung-Cheung methods for the darkness have been found to be higher than those of the illumination conditions. However, the barrier heights determined by conventional $J - V$ and Cheung-Cheung methods have been recorded to be lower and higher to the darkness and the illumination conditions, respectively. This conflict might be referred to the fact that the barrier height has been obtained from the reverse bias region of $J - V$ curve using the conventional $J - V$ method, while it has been determined from the forward bias region of $J - V$ curve by Cheung-Cheung method.

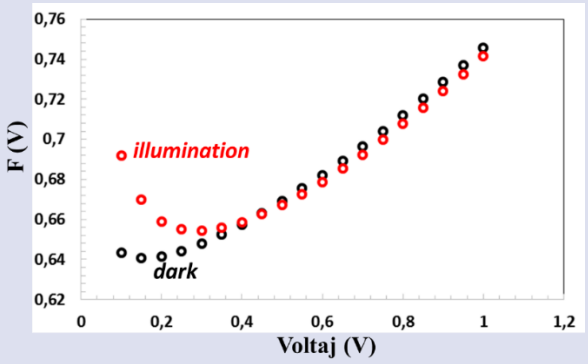

Figure 11. $F(V) - V$ characteristic of Bi doped CTS heterojunction in the darkness and the illumination.

In Fig 11, we have presented $F(V) - V$ characteristics of Bi doped CTS hetero-junction in darkness and the illumination conditions. The barrier height and serial resistance have been calculated by Norde method [41] expressed in Eq (10);

$$F(V,\gamma) = \frac{V}{\gamma} - \frac{kT}{q} ln\left(\frac{I(V)}{AA^*T^2}\right) \quad (10)$$

In Eq (10), γ is the first constant higher than ideality factor which was determined by logarithmic J-V curve. Φ_b and R_s values can be calculated by Eq (11) and Eq (12) in Norde method;

$$\Phi_b = F(V_o) + \frac{V_o}{\gamma} - \frac{kT}{q} \quad (11)$$

$$R_s = \frac{\gamma - n}{I_{min}} \frac{kT}{q} \quad (12)$$

$F(V_o)$ is the minimum value of $F(V) - V$ curve, V_o is voltage corresponding to $F(V_o)$ value, I_{min} is current corresponding to V_o value in $J - V$ curve. R_s and Φ_B values of the Bi doped CTS hetero-junction have been calculated using Eq (11) and Eq (12) to be 49.63Ω, 0.65 eV and 43.63Ω, 0.70 eV in the darkness and under the illumination conditions, respectively. R_s and Φ_B values determined by Norde method are higher than that obtained by Cheung Cheung method. The reason for this situation is that Cheung Cheung methods are only implemented to nonlinear region (in high voltage area) in forward bias of $J - V$ curve while Norde method is implemented to all forward bias region of $J - V$ curve [37].

Table 2. The photovoltaic parameters of Bi doped CTS heterojunction under the illumination

Heterojunction	J_{sc}	V_{oc}	FF	η
Bi doped CTS	0,158 mA/cm²	100 mV	0,24	0,0049 %

Bi doped CTS/n-Si heterojunction has exhibited photovoltaic behaviour as seen in logarithmic $J - V$ curve in Fig 8 and the photovoltaic parameters of the heterojunction are presented in Table 2. Since Bi doped CTS thin film has a weak crystalline structure, photo-excited charge carriers undergo more recombination [12, 42, 43]. Thus, the charge transfer to the depletion region is limited and the charge accumulation is less. This situation causes the short circuit current to be lower [30]. The photo excited charge carriers can cause leakage current at the interface. In addition, when Bi doped CTS

semiconductor with 1.55 eV band gap grown over Si semiconductor of 1.1 eV band gap, a low built in potential can occur in the depletion region [12]. Furthermore, it is also seen in Table 1 that a low barrier height is formed in the conventional $J-V$ characteristic to illumination. All these factors can lead to lower the open circuit voltage. Low J_{sc}, V_{oc} and FF values cause low power conversion efficiency. However, the work functions of n-Si semiconductor and metal contacts such as Ag, Al which are important for the contacts to exhibit ohmic property and affect photovoltaic performance of the heterojunction diode. To the metal contact to be ohmic for the n-type semiconductor, the metal's work function must be smaller than n-type semiconductor's work function ($\phi_M < \phi_S$). For a contact metal to be ohmic for a p-type semiconductor, the work function of the metal must be higher than that of the p-type semiconductor ($\phi_S < \phi_M$) [12, 44]. Al back contact (4.06 eV) tends to exhibit ohmic behaviour for n-Si (4.58 eV) semiconductors. Thus, charge flow can be easily achieved through the contact and a contribution to charge collection can be made [45-47]. As a result, Ag/Bi doped CTS/n-Si/Al hetero-junction shows the photovoltaic property and the higher efficiency can be achieved in CTS thin film solar cells with the improvement studies on CTS and Bi doped CTS thin film.

Conclusions

In this study, we have added Bi powder to Cu_xS and SnS_2 powder mixture and milled it by ball milling, and then we have produced CTS and Bi doped CTS target pellets by cold press. it has been noticed that these target pellets are Cu poor and Sn rich containing Cu_2SnS_3, Cu_2SnS_3, $Cu_2Sn_3S_7$, $Cu_4Sn_7S_{16}$ and SnS crystal phases. Bi atoms have weakened the crystal structure of CTS target pellet. However, Bi doped CTS target pellet consists of larger and homogeneously distributed particles compared to non-doped CTS target pellet. The target pellets have been ablated by laser beam and their thin films have been formed using PLD technique. CTS thin film has been produced with an amorphous structure while Bi thin film has been formed in a poor crystalline structure. These Bi doped thin films were Cu poor and Sn rich with a weak peak of SnS phase. Bi doped CTS thin film consist of larger particles compared to CTS thin film and their E_g band gap is lower than that of pure CTS thin film.

Since CTS thin film is in amorphous structure, Ag/CTS/n-Si/Al hetero-junction produced could not exhibit diode feature. On the other hand, Ag/Bi doped CTS/Si/Al hetero-junction has exhibited diode characteristics and PV behaviours. Electrical parameters of Bi doped CTS/Si hetero-junction have been calculated by the conventional $J-V$, Cheung Cheung and Norde methods in the darkness and under the illumination conditions. The ideality factors of the hetero-junction have been found somehow higher which can be attributed to the leakage current, weak crystal structure and the recombination of the charge carriers. Series resistance of the hetero-junction under the illumination conditions has been found to be lower compared to dark conditions. This situation is based on the transfer of the photo excited electron from the valence band to the conduction band which increases the number of charge carriers. The series resistance and barrier height calculated by Cheung-Cheung and Norde methods have been found to be lower and higher compared to the conventional $J-V$ method. PV parameters Bi doped CTS heterojunctions have been determined to be J_{sc}=0.158 mA/cm^2, V_{oc}=100 mV, FF=0.24 and η=0.0049%. The low power conversion efficiency of the hetero-junction device can be attributed to the leakage current, too much recombination of the charge carriers, the interface states and the low built in potential in the hetero-junction.

Acknowledgements

Authors kindly would like to thank,

- Selçuk University, High Technology Research and Application Center and

Selçuk University, *Laser Induced Proton Therapy Application and Research Center* for supplying with Infrastructure and

- Selçuk University, Scientific Research Projects Coordination (BAP) Unit for grands via projects with references of 18401178 and 20401018

Conflicts of interest

The author states that he has no conflict of interest to declare that are relevant to the content of this article.

References

[1] Berg D.M., et al., Raman analysis of monoclinic Cu2SnS3 thin films. *Applied Physics Letters*, 100(19) (20212) 192103.

[2] Bourgès C., et al., Low thermal conductivity in ternary Cu4Sn7S16 compound. *Acta Materialia*, 97 (2015) 180-190.

[3] Fu L., et al., Graphene-encapsulated copper tin sulfide submicron spheres as high-capacity binder-free anode for lithium-ion batteries. (2017).

[4] Alias M., et al., Synthesis Cu2SnS3 and Cu3SnS4 nanopowder and studying the composition, structural and morphological properties. *Journal of Non-Oxide Glasses*, 8(4) (2016) 93-97.

[5] Lokhande A., et al., Development of Cu2SnS3 (CTS) thin film solar cells by physical techniques: A status review. *Solar Energy Materials and Solar Cells*, 153 (2016) 84-107.

[6] Akaki Y., Matsuo H., Yoshino K., Structural, electrical and optical properties of Bi-doped CuInS2 thin films grown by vacuum evaporation method. *physica status solidi c*, (8) (2006) 2597-2600.

[7] Chantana J., et al., Bismuth-doped Cu (In, Ga) Se2 absorber prepared by multi-layer precursor method and its solar cell. *physica status solidi (c)*, 12(6) (2015) 680-683.

[8] Rawat K., Shishodia P., Enhancement of photosensitivity in bismuth doped Cu2ZnSnS4 thin films. P*hysica status solidi (RRL)–Rapid Research Letters,* 10(12) (2016) 890-894.

[9] Chen F.-S., et al., Cu (In, Ga) Se2 thin films codoped with sodium and bismuth ions for the use in the solar cells. *Journal of Nanomaterials,* 2015. 2015.
[10] Chalapathi U., Poornaprakash B., Park S. H., Antimony induced crystal growth for large-grained Cu2SnS3 thin films for photovoltaics. *Journal of Power Sources*, 426 (2019) 84-92.
[11] Gezgin S.Y., Kiliç H. Ş., Determination of electrical parameters of ITO/CZTS/CdS/Ag and ITO/CdS/CZTS/Ag heterojunction diodes in dark and illumination conditions. *Optical and Quantum Electronics,* 51(11) (2019) 360.
[12] Gezgin S.Y., Kılıç H. Ş., The electrical characteristics of ITO/CZTS/ZnO/Al and ITO/ZnO/CZTS/Al heterojunction diodes. *Optik*, 182 (2019) 356-371.
[13] Ettlinger R.B., et al. Pulsed laser deposition of Cu-Sn-S for thin film solar cells. in World Conference on Photovoltaic Energy Conversion 6 (2014).
[14] Zhou W., et al., Sustainable thermoelectric materials fabricated by using Cu2Sn1-x Zn x S3 nanoparticles as building blocks. *Applied Physics Letters*, 111(26) (2017) 263105.
[15] Chen X., et al., SnS/N-Doped carbon composites with enhanced Li+ storage and lifetime by controlled hierarchical submicron-and nano-structuring. *CrystEngComm*, 22(9) (2020) 1547-1554.
[16] Hossain E.S., et al., Fabrication of Cu2SnS3 thin film solar cells by sulphurization of sequentially sputtered Sn/CuSn metallic stacked precursors. *Solar Energy*, 177 (2019) 262-273.
[17] Wang C.-J., et al., Fabrication and sulfurization of Cu2SnS3 thin films with tuning the concentration of Cu-Sn-S precursor ink. *Applied Surface Science*, 388 (2016) 71-76.
[18] He T., et al., The role of excess Sn in Cu 4 Sn 7 S 16 for modification of the band structure and a reduction in lattice thermal conductivity. *Journal of Materials Chemistry C,* 5(17) (2017) 4206-4213.
[19] Cui J., et al., Improved thermoelectric performance of solid solution Cu 4 Sn 7.5 S 16 through isoelectronic substitution of Se for *S. Scientific reports*, 8(1) (2018) 1-9.
[20] Weber A., Mainz R., Schock H., On the Sn loss from thin films of the material system Cu–Zn–Sn–S in high vacuum. *Journal of Applied Physics*, 107(1) (2010) 013516.
[21] Jackson A.J., Walsh A., Ab initio thermodynamic model of Cu 2 ZnSnS 4. *Journal of Materials Chemistry A*, 2(21) (2014) 7829-7836.
[22] Berg D.M., et al., Thin film solar cells based on the ternary compound Cu2SnS3. *Thin Solid Films*, 520(19) (2012) 6291-6294.
[23] Andrade Jr, M.A., Mascaro L. H., Bismuth doping on CuGaS2 thin films: structural and optical properties. *MRS COMMUNICATIONS*, 8(2) (2018) 504.
[24] Liu N., et al., Synthesis and characterization of (Cu 1− x Ag x) 2 ZnSnS 4 nanoparticles with phase transition and bandgap tuning. *Journal of Materials Science: Materials in Electronics*, (2020) p. 1-9.
[25] Zhao Y., et al., Effect of Ag doping on the performance of Cu2SnS3 thin-film solar cells. *Solar Energy,* 201 (2020) 190-194.
[26] Alijani M., Ilkhechi N. N., Effect of Ni Doping on the Structural and Optical Properties of TiO 2 Nanoparticles at Various Concentration and Temperature. *Silicon*, 10(6) (2018) 2569-2575.
[27] Ammar I., Gassoumi A., Turki-Kamoun N., The Effect of TSC and Nickel Doping on SnS Thin Films. Silicon, 2020: p. 1-6.
[28] Song N., et al., Epitaxial Cu2ZnSnS4 thin film on Si (111) 4 substrate. Applied Physics Letters, 106(25) (2015) 252102.
[29] Shin B., et al., Epitaxial growth of kesterite Cu2ZnSnS4 on a Si (001) substrate by thermal co-evaporation. T*hin Solid Films,* 556 (2014). 9-12.
[30] Gezgin S.Y., Houimi A., Kılıç H. Ş., Production and photovoltaic characterisation of n-Si/p-CZTS heterojunction solar cells based on a CZTS ultrathin active layers. *Optik*, 199 (2019) 163370.
[31] Jia Z., et al., The photovoltaic properties of novel narrow band gap Cu 2 SnS 3 films prepared by a spray pyrolysis method. *RSC Advances,* 5(37) (2015) 28885-28891.
[32] Welatta F., et al. Fabrication and characterization of copper-tin-sulfide thin film. *in AIP Conference Proceedings*. (2018) AIP Publishing LLC.
[33] Uslu H., et al., The interface states and series resistance effects on the forward and reverse bias I–V, C–V and G/ω-V characteristics of Al–TiW–Pd2Si/n-Si Schottky barrier diodes. *Journal of alloys and compounds*, 503(1) (2010) 96-102.
[34] Elhouichet H., Othmen W. B. H., Dabboussi S., Effect of Sb, Tb 3+ Doping on Optical and Electrical Performances of SnO 2 and Si Based Schottky Diodes. *Silicon*, 12(3) (2020) 715-722.
[35] Tataroğlu A., Altındal Ş., Azizian-Kalandaragh y., Electrical and photoresponse properties of CoSO.
[36] Lambada D.R., et al., Investigation of Illumination Effects on the Electrical Properties of Au/GO/p-InP Heterojunction with a Graphene Oxide Interlayer. *Nanomanufacturing and Metrology*, (2020) 1-13.
[37] Özerli H., et al., Electrical and photovoltaic properties of Ag/p-Si structure with GO doped NiO interlayer in dark and under light illumination. *Journal of Alloys and Compounds*, 718 (2017). 75-84.
[38] Soliman H., et al., Electronic and photovoltaic properties of Au/pyronine G (Y)/p-GaAs/Au: Zn heterojunction. *Journal of alloys and compounds,* 530 (2012) 157-163.
[39] Karataş Ş., Yakuphanoğlu F., Effects of illumination on electrical parameters of Ag/n-CdO/p-Si diode. *Materials Chemistry and Physics*, 138(1) (2013) 72-77.
[40] Bedia F., et al., Electrical characterization of n-ZnO/p-Si heterojunction prepared by spray pyrolysis technique. *Physics Procedia*, 55 (2014) 61-67.
[41] Norde H., A modified forward I-V plot for Schottky diodes with high series resistance. *Journal of Applied Physics,* 50(7) (1979) 5052-5053.
[42] Shi Z., Jayatissa A. H., One-pot hydrothermal synthesis and fabrication of kesterite Cu2ZnSn (S, Se) 4 thin films. *Progress in Natural Science: Materials International*, 27(5) (2017) 550-555.
[43] Zedan I., El-Menyawy E., Mansour A., Physical Characterizations of 3-(4-Methyl Piperazinylimino Methyl) Rifampicin Films for Photodiode Applications. *Silicon*, 11(3) (2019) 1693-1699.
[44] Gezgin S.Y., Kiliç H. Ş., Determination of electrical parameters of ITO/CZTS/CdS/Ag and ITO/CdS/CZTS/Ag heterojunction diodes in dark and illumination conditions. *Optical and Quantum Electronics*, 51(11) (2019) 1-22.
[45] Yao Z., et al., High-Performance and Stable Dopant-Free Silicon Solar Cells with Magnesium Acetylacetonate Electron-Selective Contacts. *physica status solidi (RRL)–Rapid Research Letters*, 14(6) (2020) 2000103.
[46] Kang J., et al., Electron-Selective Lithium Contacts for Crystalline Silicon Solar Cells. *Advanced Materials Interfaces*, (2021) 2100015.
[47] Ali M., et al., Optimization Of Monoclinic Cu2sns3 (Cts) Thin Film Solar Cell Performances Through Numerical Analysis. *Chalcogenide Letters*, 17(2) (2020) 85-98.